TECHNICAL NOTE

Bearing Capacity of Cylindrical Caissons in Cohesive-Frictional Soils Using Axisymmetric Finite Element Limit Analysis

Suraparb Keawsawasvong · Jim Shiau ·
Kittiphan Yoonirundorn

Abstract This paper investigates the use of stability factors for estimating the ultimate bearing pressures on cylindrical caissons in cohesive-frictional soils. Rigorous upper and lower bound limit analyses with finite elements in axisymmetric (AX) condition are used for a series of numerical studies. The bearing capacity factors (N_{c0}, N_{q0} and $N_{\gamma0}$) for a surface circular footing are firstly revisited. This is followed by a study on the effect of caisson's embedded depth ratio (L/D). A comprehensive set of depth factors (F_{cd}, F_{qd} and $F_{\gamma d}$) is then reported as a function of caisson's embedded depth ratio (L/D) and soil internal friction angle (ϕ). The obtained results are compared with published solutions in the literature. Several examples are given to validate the principal of superposition as well as to illustrate on how to use the produced factors to estimate the ultimate bearing pressures on cylindrical caissons in cohesive-frictional soils. The study should be of great interests to practitioners.

1 Introduction

Cylindrical caissons, also known as skirted or bucket foundations, have been proven to be an effective foundation system for bridges, piers, floating platforms and other offshore foundations in deep water (Deng et al. 2020; Mello et al. 2021; Sales et al. 2021). Caisson is generally made from a large steel thin-walled cylindrical structure that is open at the bottom and closed at the top. A comprehensive review of the offshore foundation was presented in Randolph and Gourvenec (2011), who reported that the depth ratio between the diameter and the depth of caissons is in the range of 1–6.

Early studies on the behaviour of caissons in cohesive soils were conducted by using field experiments and centrifuge model tests (Andersen et al. 1993; Dyvik et al. 1993; Clukey and Morrison 1993; Cauble 1996). Numerical methods such as using the displacement-based finite element and the finite element limit analysis were also reported by numerous researchers (see e.g., Bransby and Yun 2009; Geer 1996; Gourvenec 2008; Gourvenec and Barnett 2011; Mana et al. 2013; Ukritchon et al. 2018; Keawsawasvong et al. 2021; Keawsawasvong and Lawongkerd 2021; Keawsawasvong and Ukritchon 2016; Ukritchon and

S. Keawsawasvong (✉) · K. Yoonirundorn
Department of Civil Engineering, Thammasat
School of Engineering, Thammasat University,
Pathumthani 12120, Thailand
e-mail: ksurapar@engr.tu.ac.th

J. Shiau
School of Civil Engineering and Surveying, University
of Southern Queensland, Toowoomba, QLD, Australia

Keawsawasvong 2016; Yun and Bransby 2007). Most of the research work done was for the bearing and pull-out capacity of caissons in undrained clays. Very few works were reported in relation to soils in drained condition. In addition, the studies on the behaviours of open caissons were also considered by Lai et al. (2020, 2021) and O'Dwyer et al. (2018, 2020).

The bearing capacity of strip foundations with structural skirts was presented by Al-Aghbari and Mohamedzein (2004) who performed a series of model tests on these footings embedded in dense sand. Later, Al-Aghbari and Dutta (2008) and Eid et al. (2009) conducted several experiments to investigate the behaviours of square skirted footings in sand. A numerical finite element analysis was employed by Eid (2013) to evaluate the bearing capacity and settlement of skirted shallow foundations on sand. The effect of different types of sands (e.g., medium dense and dense sands) on the bearing capacity of circular skirted footings in sand was examined by Wakil (2013). Khatri et al. (2017) later performed a series of small-scale model test to study the behaviour of rectangular and square skirted footings on sand. Using the finite element limit analysis (FELA), Khatri and Kumar (2019) proposed the depth factor for soil weight $F_{\gamma d}$ for circular and strip skirted footings with small embedment depth ratios (L/D) varying from 0 to 2.

Very recently, Shiau and Al-Asadi (2020a, b) adopted a stability factor approach, that is analogous to the traditional bearing capacity problem, to study the drained stability solutions of underground tunnelling. The method has been proven to be both efficient and effective. So far, there is no comprehensive results of the depth factors (F_{cd}, F_{qd} and $F_{\gamma d}$) for the caisson problems in the literature. Following the stability factor approach in Shiau and Al-Asadi (2020c), the focus of this study is to assess the ultimate bearing pressures on cylindrical caissons in cohesive-frictional soils using the advanced upper and lower bound limit analysis. Comprehensive bearing capacity factors (N_{c0}, N_{q0} and $N_{\gamma 0}$) and depth factors (F_{cd}, F_{qd} and $F_{\gamma d}$) are presented in tables and figures to assist designers and practising engineers in calculating the critical pressure that can apply to the caissons in their preliminary stage of design. Note that the bearing capacity factors (N_{c0}, N_{q0} and $N_{\gamma 0}$) are used for the cases of circular footings resting on the surface of soils. To consider the circular skirted footings

with an embedment depth ($L/D > 0$), the depth factors (F_{cd}, F_{qd} and $F_{\gamma d}$) are then adopted. This will be demonstrated in the example section of the paper.

2 Stability Factor Approach

The problem definition of a cylindrical caisson in axisymmetry (AX) for a cohesive-frictional soil is shown in Fig. 1. The caisson has a diameter D and an embedment depth L. The ground surface is subject to a vertical surcharge (q), while a bearing pressure at the top of the caisson is (q_u). The soil medium obeys the Mohr–Coulomb failure criterion with three parameters including cohesion (c), unit weight (γ), and friction angle (ϕ).

Terzaghi's bearing capacity equation, as shown in Eq. (1), can be used to calculate the ultimate uniform pressure q_u applied at the top cap of a 2D plane strain caisson when $L = 0$.

$$q_u = cN_c + qN_q + 0.5\gamma D N_\gamma \tag{1}$$

where c is the soil cohesion; q is the surcharge loading; γ is the soil unit weight; N_c is the 2D plane strain bearing capacity factor for cohesion; N_q is the 2D plane strain bearing capacity factor for surcharge
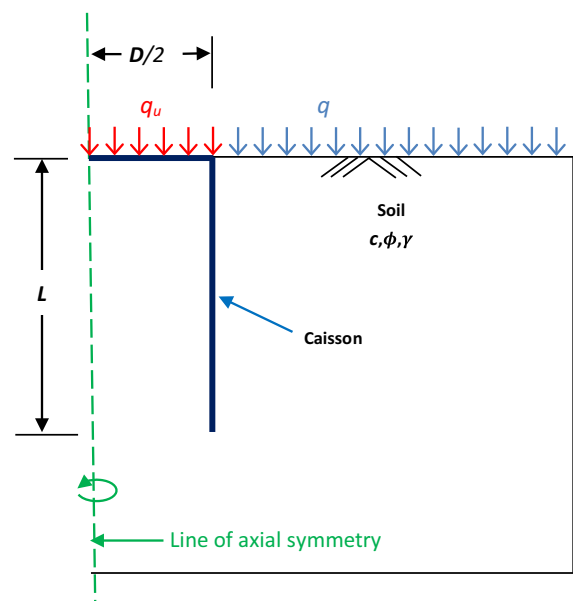

Fig. 1 The axisymmetric problem of a caisson

loading; N_γ is the 2D plane strain bearing capacity factor for soil weight.

Equation (1) is further modified to Eq. (2) to include the axisymmetric effects in 3D using (N_{c0}, N_{q0} and $N_{\gamma0}$) as well as the depth factor (L/D) effects using (F_{cd}, F_{qd} and $F_{\gamma d}$).

$$q_u = cN_{c0}F_{cd} + qN_{q0}F_{qd} + 0.5\gamma DN_{\gamma0}F_{\gamma d} \qquad (2)$$

where (N_{c0}, N_{q0}, and N_{q0}) are the axisymmetric bearing capacity factors for cohesion, surcharge, and soil weight respectively of a surface circular footing ($L/D = 0$). The three bearing capacity factors (N_{c0}, N_{q0} and $N_{\gamma0}$) are a function of only soil internal friction angle (ϕ). On the other note, the depth factors (F_{cd}, F_{qd} and $F_{\gamma d}$) of cylindrical caissons are a function of both the soil internal friction angle (ϕ) and the depth ratio (L/D) of the caissons. Interestingly, the three depth factors are unity when $L/D = 0$, and Eq. (2) reduces to Eq. (3) for the problem of surface circular footings.

$$q_u = cN_{c0} + qN_{q0} + 0.5\gamma DN_{\gamma0} \qquad (3)$$

As stated in Shiau and Al-Asadi (2020b), to obtain the respective factors such as (N_{c0}, $N_{q0,}$ and $N_{\gamma0}$) and (F_{cd}, $F_{qd,}$ and $F_{\gamma d}$), it is necessary to impose zero value to c (cohesion) or q (surcharge) or γ (soil unit weight). This procedure works well to obtain individual pressure q_u for cohesion, surcharge, and unit weight. They are then used to calculate the respective factor of a given depth ratio (L/D). The factor N_{c0} can be obtained by assuming no surface pressure ($q = 0$) and weightless soil ($\gamma = 0$) whereas the factor N_{q0} be acquired by assuming no cohesion ($c = 0$) and weightless soil ($\gamma = 0$). In addition, the factor $N_{\gamma0}$ can also be obtained by assuming no cohesion ($c = 0$) and surface pressure ($q = 0$). The principal of superposition has been discussed and validated by Shiau and Al-Asadi (2020a), and in this paper again, has been successfully applied to the examples in a later section.

3 FELA Model

Recent advances in Finite Element Limit Analysis (*FELA*) with both upper bound (*UB*) and lower bound (*LB*) estimates are powerful as they can provide an error indicator towards the true collapse load (Sloan 2013). The development began with linear programming in Sloan (1988, 1989). Nonlinear programming formulations provide better solution accuracy with shorter cpu solution time (Lyamin and Sloan 2002a, b; Krabbenhoft et al. 2007). Recently, the *FELA* (Optum CE 2021) has been widely used to solve a variety of drained and undrained stability problems in geotechnical engineering (Shiau and Smith 2006, Shiau et al. 2016a, b, c, 2021a, b; Shiau and Al-Asadi 2020c, d, 2021; Keawsawasvong and Ukritchon 2017a, b, 2020, 2021; Ukritchon and Keawsawasvong 2017a, b, 2019a, b, 2020a, b; Ukritchon et al. 2019, 2020; Yodsomjai et al. 2021) and it was chosen in this study to compute the bearing capacity factors (N_{c0}, N_{q0} and $N_{\gamma0}$) and the depth factors (F_{cd}, F_{qd} and $F_{\gamma d}$) of the cylindrical caissons in axisymmetric condition.

In the LB method, three-node triangular elements are used in the analysis. Each triangular element has the nodal stresses of σ_r, σ_z, σ_θ, and τ_{rz} for an axisymmetric problem. The statically admissible stress discontinuities are allowed for producing the continuity of normal and shear stresses along with the interfaces of all the elements. The conditions of stress equilibrium, stress boundary condition, and the Mohr–Coulomb failure criterion are the constraints in a typical LB analysis, in which the objective function is to maximize the collapse load of problems. On the other hand, the upper bound theorem requires a kinematically admissible velocity field where the external work is greater or equal to the plastic shear dissipation. In the UB method, three-node triangular elements are used in the formulation. At each node of the element, there are the horizontal (u) and vertical velocities (v) defined as the basic unknown variables. The setting of kinematically admissible velocity discontinuities is applied at the interfaces of all the elements. The material is set to obey the associated flow rule. These two theorems are perfectly fitted to the nonlinear programming optimization problems using the second-order cone programming (SOCP). The constraints involved in this procedure are nonlinear and non-smooth but remain convex and amenable to analysis.

Since the problem of an cylindrical caisson can be modelled under an axisymmetric (AX) condition, only half of the domain is employed in the simulation, as shown in Fig. 2. The line of axial symmetry is set to be located at the left of the domain. Noting that the underlying bound
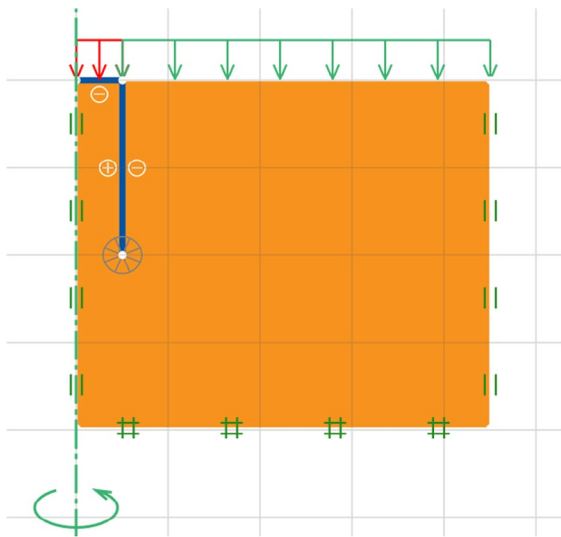
Fig. 2 Numerical model under an axisymmetric condition in OptumG2

Fig. 3 A typical mesh for F_{cd} solution ($L/D=2$). **a** Initial setting with 5,000 elements; **b** final setting with 10,000 elements

theorems assume a rigid-perfectly plastic material with associated plasticity, the soil mass is discretised as triangular elements and modelled as Mohr–Coulomb material. The caisson is modelled by using rigid plate elements. The interface condition at the contact surface between the caisson and the soil is set to be fully rough. The feature "*Fan Mesh*" in the program is activated at the tip of the caisson to improve the solution accuracy (Krabbenhoft et al. 2015). The bottom boundary of the model is fixed in both horizontal and vertical directions, while the left and the right boundary can move in the vertical direction. The domain size was chosen to be large enough so that the solution is not affected by the development of the overall velocity field.

An automatically adaptive mesh refinement was employed in both the *UB* and *LB* simulations to compute the tight *UB* and *LB* solutions of the ultimate pressure q_u. Figure 3 presents a typical example of the mesh refinement technique for a depth ratio of ($L/D)=2$. The initial *FELA* mesh with approximately 5,000 elements is shown in Fig. 3a, whilst the final mesh with 10,000 elements is shown in Fig. 3b. It should be also noted that all presented numerical results hereafter are the average solutions from *LB* and *UB FELA* after the five
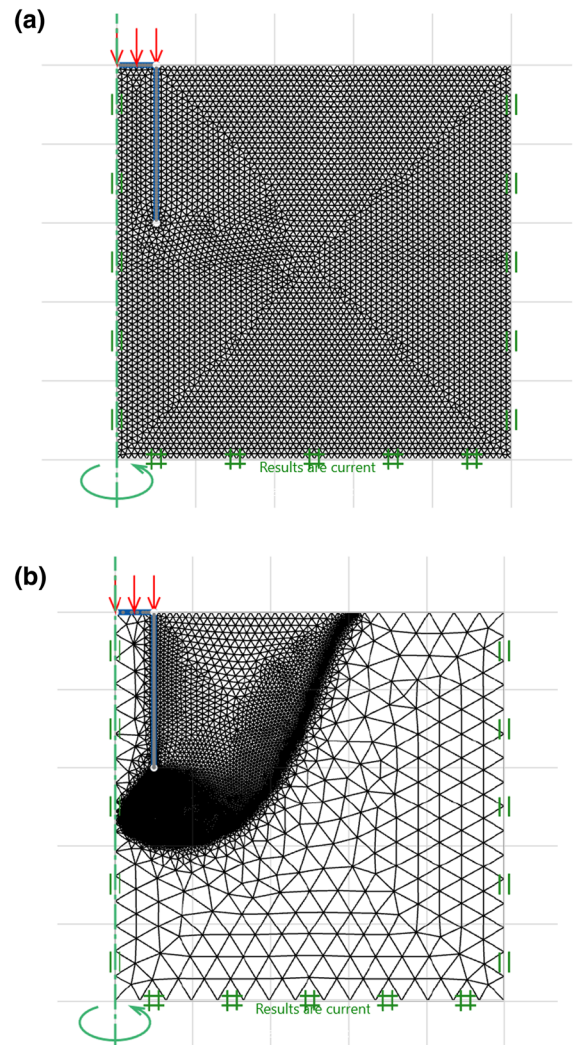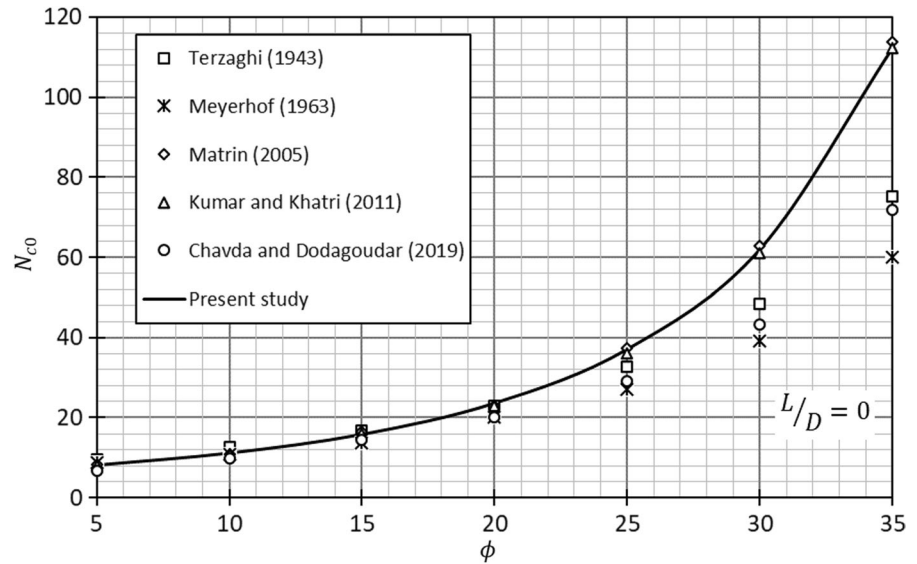
adaptive mesh refinement steps with approximately 10,000 elements.

4 Discussing the Axisymmetric Factors N_{c0}, N_{q0}, and $N_{\gamma0}$

Numerical results of the axisymmetric (AX) cohesion factor N_{c0} ($L/D=0$) with soil frictional angles ϕ varying from 5° to 35° are presented in Fig. 4. Noting that N_{c0} increases nonlinearly with the increasing ϕ, they are in excellent agreement with the slip line solutions in Martin (2004) and Kumar and Khatri (2011). As

Fig. 4 Variation and comparison of N_{c0} with ϕ for surface cylindrical caissons ($L/D = 0$)

discussed in Sloan (2013), the slip line solutions by Martin (2004) can be considered as nearly exact solutions. The published N_{c0} results of Terzaghi (1943), Meyerhof (1963), and the displacement-based finite element of Chavda and Dodagoudar (2019) are consistently lower than those in the present study and they are considered as conservative solutions.

Figure 5 presents numerical results of the axisymmetric (AX) surcharge factor N_{q0} ($L/D = 0$) with ϕ varying from 5° to 35°. Similar trends as in the cohesion factor N_{c0}, the nonlinearly increasing results have

compared well with published ones, except those conservative solutions of Terzaghi (1943), Meyerhof (1963) and Chavda and Dodagoudar (2019). For the axisymmetric (AX) soil unit weight factor $N_{\gamma0}$ ($L/D = 0$), again, numerical results in Fig. 6 have suggested great confidence in using the present averaged results of rigorous upper and lower bounds. Interestingly, the finite difference results reported by Zhao and Wang (2008) are unsafe (or unconservative) as they are consistently greater than our solutions. The values of N_{c0}, $N_{q0,}$ and $N_{\gamma0}$ are explicitly shown

Fig. 5 Variation and comparison of N_{q0} with ϕ for surface cylindrical caissons ($L/D = 0$)
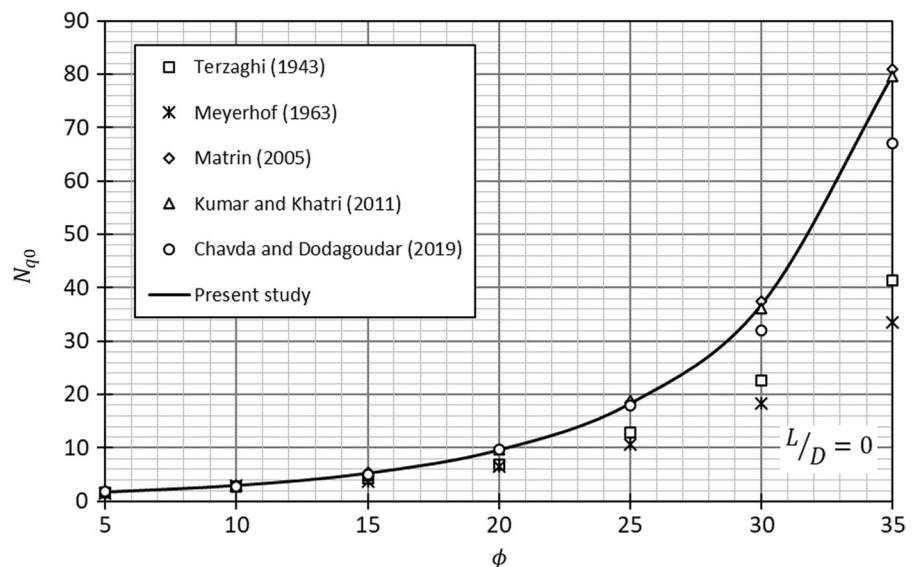
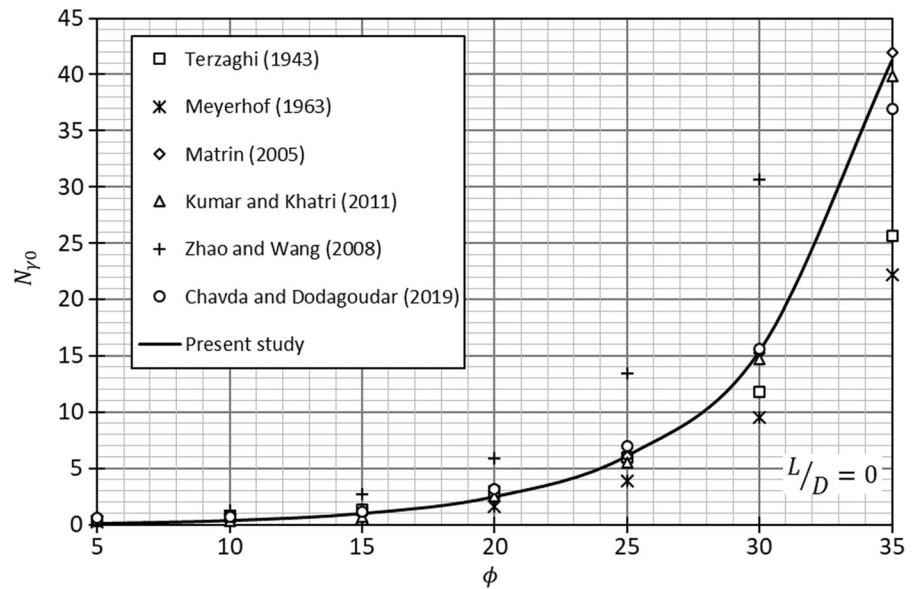**Fig. 6** Variation and comparison of $N_{\gamma 0}$ with ϕ for surface cylindrical caissons ($L/D = 0$)

Table 1 Axisymmetric bearing capacity factors N_{c0}, N_{q0} and $N_{\gamma 0}$ ($L/D = 0$)

ϕ (°)	N_{c0}	N_{q0}	$N_{\gamma 0}$
5	8.035	1.712	0.118
10	11.053	2.962	0.379
15	15.732	5.247	1.008
20	23.546	9.602	2.506
25	37.050	18.324	6.145
30	62.000	36.885	15.469
35	112.409	79.893	41.298

in Table 1. It should be noted that the all presented results are in good accordance with the research of Kumar and Khatri (2011) since this study and Kumar and Khatri (2011) employed the same FELA method to solve the solutions of circular foundation problems. However, Kumar and Khatri (2011) only proposed the bearing capacity factors for surface circular foundations. The solutions of caissons with a given depth ratio (L/D) have never been presented in the past. To the best of our knowledge, this study is the first work to consider the depth factors F_{cd}, F_{qd}, and $F_{\gamma d}$ for the caisson problem.

5 Discussing the Depth Factors F_{cd}, F_{qd}, and $F_{\gamma d}$

Numerical solutions of the axisymmetric (AX) cohesion depth factor F_{cd} with soil frictional angles ϕ varying from 5° to 35° are presented in Fig. 7 for ($L/D = 0$ to 6). The value of F_{cd} starts from one at $L/D = 0$, and it increases linearly with the increase in L/D for all considered fiction angles $\phi = 5°$ to 35°. The larger the ϕ, the greater the F_{cd}. The effect of ϕ is insignificant when $\phi > 30°$ since both lines of $\phi = 30°$ and 35° overlap perfectly.

Figure 8 shows that, for all friction angles, the surcharge depth factor F_{qd} increases as L/D increases. This increase is approximately linear. The deeper the caisson is, the larger the F_{qd} (surcharge effect) is. The greater the ϕ, the larger the F_{qd}. For the soil unit weight depth factor $F_{\gamma d}$, see Fig. 9, a highly nonlinear relationship between $F_{\gamma d}$ and L/D is observed. An increase in L/D yields an increase in $F_{\gamma d}$. Noting that $F_{\gamma d}$ is the smallest when $\phi = 35°$, whilst the largest when $\phi = 5°$. This is dissimilar to the other factors such as F_{cd} and F_{qd}. A possible explanation for this might be due to the local punching failure mechanism near the end bearing point of the deep foundation. The complete values of (F_{cd}, F_{qd}, and $F_{\gamma d}$) are explicitly presented in Tables 2, 3 and 4. Using the bearing capacity factors (N_{c0}, N_{q0}, and $N_{\gamma 0}$) and the depth factors (F_{cd}, F_{qd}, and $F_{\gamma d}$), Eq. (2) can be used by

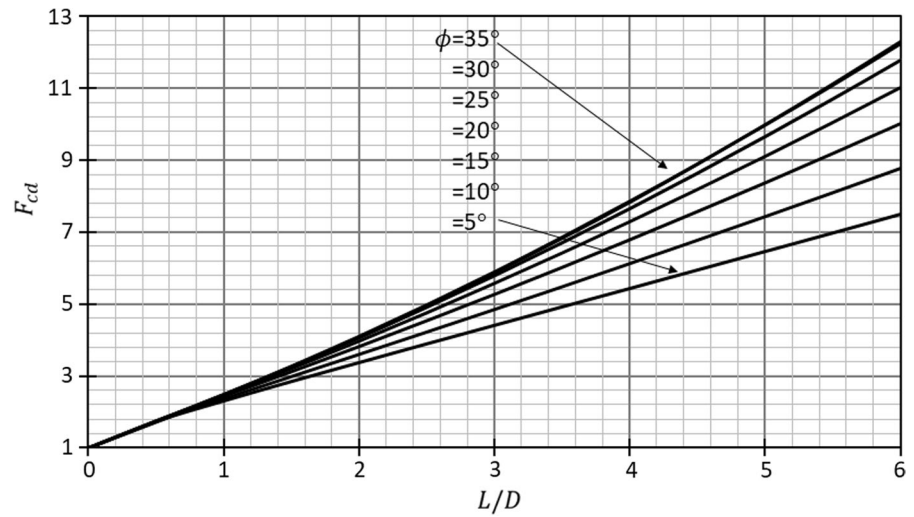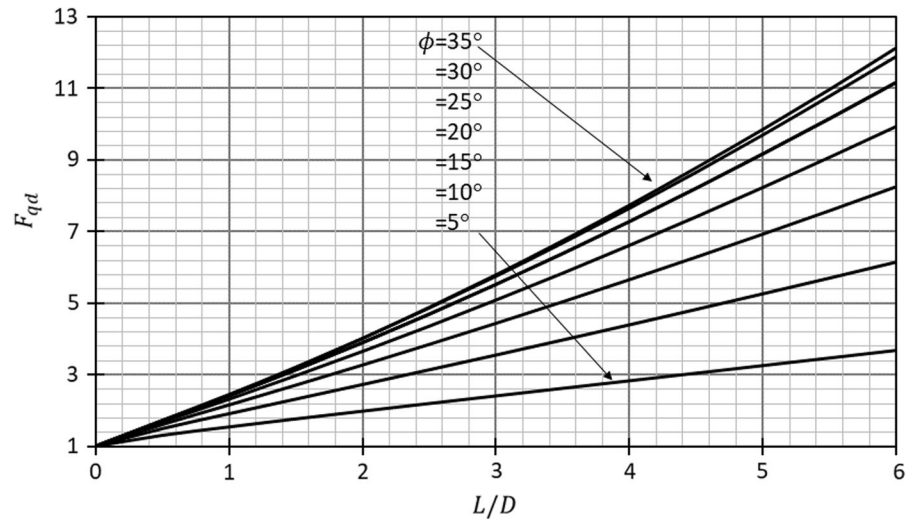**Fig. 7** The depth factor for cohesion F_{cd} with various L/D and ϕ

Fig. 8 The depth factor for surcharge F_{qd} with various L/D and ϕ

practical engineers to evaluate the ultimate capacity q_u of cylindrical caissons in cohesive-frictional soils.

Figure 10 compares the unit weight depth factor $F_{\gamma d}$ between the present study and the footing embedment study by Lyamin et al. (2007), as well as the study of skirt foundation on the sand by Khatri and Kumar (2019). Note that the work by Khatri and Kumar (2019) was for cylindrical skirt footings with the soils inside the skirt, whereas Lyamin et al. (2007) studied rigid embedded footings without the soils inside. The comparison shows a good agreement between the present results with those in Khatri and Kumar (2019). Though not entirely the same as our current study, the solutions provided by Lyamin et al. (2007) are conservative as they predict lower $F_{\gamma d}$ factors than those in Khatri and Kumar (2019) and in this study.

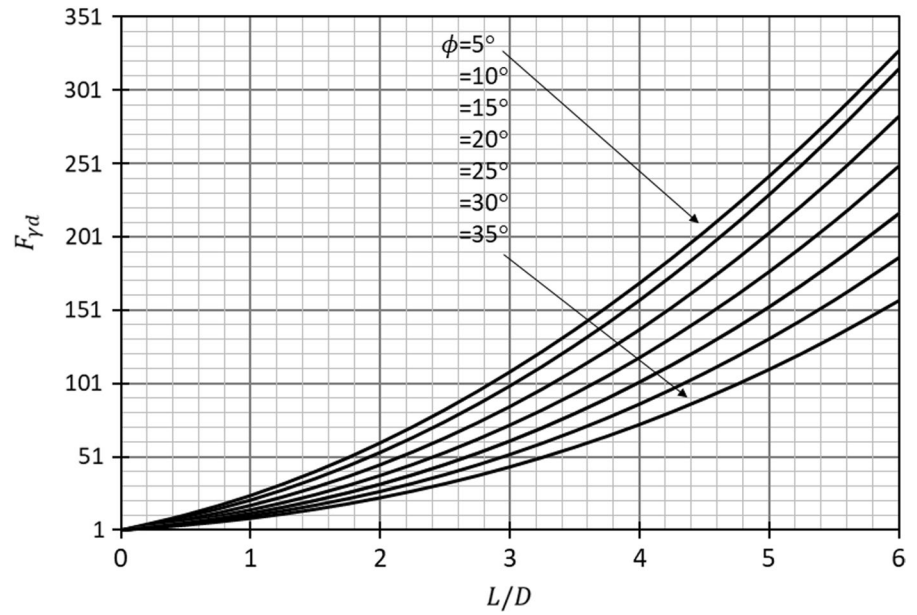**Fig. 9** The depth factor for unit weight $F_{\gamma d}$ with various L/D and ϕ

Table 2 The depth factor for cohesion F_{cd}

ϕ (°)	L/D												
	0	0.5	1	1.5	2	2.5	3	3.5	4	4.5	5	5.5	6
5	1.000	1.736	2.309	2.850	3.375	3.894	4.408	4.922	5.433	5.945	6.461	6.975	7.493
10	1.000	1.741	2.372	2.989	3.604	4.226	4.852	5.485	6.130	6.778	7.436	8.101	8.775
15	1.000	1.754	2.436	3.121	3.821	4.536	5.267	6.018	6.785	7.568	8.365	9.181	10.010
20	1.000	1.754	2.470	3.206	3.969	4.758	5.575	6.418	7.287	8.184	9.101	10.043	11.011
25	1.000	1.750	2.489	3.258	4.068	4.911	5.789	6.704	7.652	8.635	9.651	10.698	11.774
30	1.000	1.743	2.488	3.273	4.105	4.977	5.893	6.855	7.854	8.890	9.966	11.075	12.224
35	1.000	1.722	2.454	3.232	4.062	4.940	5.865	6.835	7.837	8.893	9.994	11.128	12.302

Table 3 The depth factor for surcharge F_{qd}

ϕ (°)	L/D												
	0	0.5	1	1.5	2	2.5	3	3.5	4	4.5	5	5.5	6
5	1.000	1.305	1.543	1.767	1.986	2.201	2.415	2.628	2.841	3.055	3.268	3.481	3.695
10	1.000	1.490	1.907	2.315	2.723	3.134	3.548	3.968	4.392	4.822	5.258	5.698	6.144
15	1.000	1.605	2.154	2.708	3.272	3.849	4.439	5.043	5.662	6.293	6.938	7.594	8.265
20	1.000	1.674	2.315	2.974	3.656	4.361	5.094	5.847	6.627	7.426	8.249	9.094	9.959
25	1.000	1.709	2.405	3.134	3.897	4.693	5.525	6.389	7.285	8.213	9.175	10.164	11.180
30	1.000	1.709	2.405	3.134	3.897	4.693	5.525	6.389	7.285	8.213	9.175	10.164	11.180
35	1.000	1.713	2.432	3.201	4.017	4.885	5.796	6.751	7.746	8.793	9.868	10.988	12.153

Table 4 The depth factor for unit weight $F_{\gamma d}$

ϕ (°)	L/D												
	0	0.5	1	1.5	2	2.5	3	3.5	4	4.5	5	5.5	6
5	1.000	11.492	24.703	41.093	60.636	83.280	109.034	137.814	169.661	204.585	242.661	283.763	328.186
10	1.000	10.235	21.588	36.293	54.113	75.169	99.456	127.050	157.992	192.243	230.018	271.282	315.858
15	1.000	8.339	17.942	30.321	45.631	63.959	85.353	110.002	137.756	168.997	203.715	241.617	283.114
20	1.000	6.976	14.920	25.289	38.359	54.075	72.711	94.239	118.775	146.541	177.443	211.689	249.449
25	1.000	5.940	12.561	21.352	32.404	45.882	61.914	80.613	102.138	126.377	153.511	183.894	217.165
30	1.000	5.127	10.687	18.067	27.410	38.920	52.560	68.557	86.959	107.894	131.403	157.569	186.619
35	1.000	4.474	9.131	15.320	23.149	32.779	44.239	57.689	73.189	90.925	110.747	133.028	157.678

Fig. 10 Comparison of $F_{\gamma d}$

6 Examples

Several examples are presented in this section to demonstrate how to use the produced results to evaluate the uniform bearing capacity of cylindrical caissons by using the formulation shown in Eq. (2). The principal of superposition using the stability factor approach is also validated with the following examples.

6.1 Example 1: Cohesionless Soil Without Surcharge Loading

A cylindrical caisson has the length $L = 12$ m and the diameter $D = 3$ m. The design parameters are given as: the unit weight $\gamma = 18$ kPa and the soil internal friction angle $\phi = 35°$. The soil cohesion c is zero since the soil is cohesionless. The surcharge loading q is also zero in this example. Given $\phi = 35°$, the value of $N_{\gamma 0} = 41.298$ is obtained from Table 1 and $F_{\gamma d} = 73.189$ is also obtained from Table 4 using $L/D = 4$. Note that the values of N_{c0}, N_{q0}, F_{cd} and F_{qd} are not required since $c = 0$ kPa and $q = 0$ kPa. Using Eq. 2, the ultimate uniform

pressure can be then calculated as: $q_u = (0.5 \times 18 \times 3 \times 41.298 \times 73.189) = 81,609.10$ kPa.

An actual computer analysis of the problem gives $q_u = 81,672.279$ kPa, which is very close to the solution using stability factors and the principal of superposition.

6.2 Example 2: Cohesionless Soil with Surcharge Loading

Same as in Example 1, now the surcharge loading $q = 20$ kPa. From Table 1, given $\phi = 35°$, the values of $N_{q0} = 79.893$ and $N_{\gamma 0} = 41.298$. The values of $F_{qd} = 7.746$ and $F_{\gamma d} = 73.189$ can also be obtained from Tables 3 and 4 respectively for $\phi = 35°$ and $L/D = 4$. Note that the values of N_{c0} and F_{cd} are not required since $c = 0$ kPa in this example. Using Eq. 2, the ultimate uniform pressure can be then calculated as: $q_u = [(20 \times 79.893 \times 7.746) + (0.5 \times 18 \times 3 \times 41.298 \times 73.189)] = 93,986.13$ kPa.

An actual analysis in the program using the real parameters gives $q_u = 95,164.657$ kPa, which is 1.2% greater than the solution using stability factors and the principal of superposition.

6.3 Example 3: Cohesive-Frictional Soil Without Surcharge Loading

In this example, the cylindrical caisson has a diameter $D = 4$ m (i.e. $L/D = 3$). The design parameters are given as the unit weight $\gamma = 16$ kPa, the soil internal friction angle $\phi = 10°$, and the soil cohesion $c = 25$ kPa. There is no surcharge loading at the ground surface so that $q = 0$ kPa. From Table 1, given $\phi = 10°$, the values of $N_{c0} = 11.053$ and $N_{\gamma 0} = 0.379$ are obtained. The values of $F_{cd} = 4.852$ and $F_{\gamma d} = 99.456$ are also obtained from Tables 2 and 4 respectively for $\phi = 10°$ and $L/D = 3$. Note that the values of N_{q0} and F_{qd} are not required since $q = 0$ kPa. Using Eq. 2, the ultimate uniform pressure can be then calculated as: $q_u = [(25 \times 11.053 \times 4.852) + (0.5 \times 16 \times 4 \times 0.379 \times 99.456)] = 2,546.93$ kPa. An actual computer analysis of the problem gives $q_u = 2,567.307$, which is very close to the solution using stability factors and the principal of superposition.

The above examples have proven that the principal of superposition with the stability factors and the depth factors can be used to evaluate the unltimate bearing pressures of caissons.

7 Conclusions

This paper has successfully produced lower and upper bound solutions of the bearing capacity factors (N_{c0}, N_{q0}, and $N_{\gamma 0}$) and the depth factors (F_{cd}, F_{qd}, and $F_{\gamma d}$) for cylindrical caissons in cohesive-frictional soil. The following conclusions are drawn based on this study:

1. The axisymmetric bearing capacity factors (N_{c0}, N_{q0}, and $N_{\gamma 0}$) for a surface footing are a function of only the soil friction angle (ϕ). An increase in the soil friction angle (ϕ) results in an increase in all three bearing capacity factors (N_{c0}, N_{q0}, and $N_{\gamma 0}$).

2. The depth factors (F_{cd}, F_{qd}, and $F_{\gamma d}$) are functions of both the soil friction angle (ϕ) and the depth ratio (L/D). An increase in the depth ratio (L/D) causes an increase in all depth factors (F_{cd}, F_{qd}, and $F_{\gamma d}$).

3. For the unit weight depth factor, $F_{\gamma d}$, an increase in the soil friction angle (ϕ) results in a decrease in $F_{\gamma d}$. This is different from F_{cd} and F_{qd}, where they increase with the increasing soil friction angle (ϕ). A possible explanation for this might be due to the local punching failure near the end bearing point of the foundation.

4. The present solutions of bearing capacity factors (N_{c0}, N_{q0}, and $N_{\gamma 0}$) are in good agreement with the previous solutions using the method of characteristic. In addition, the present solutions of the depth factor $F_{\gamma d}$ are also in good agreement with those published ones.

5. The illustrated examples using the principal of superposition have proven that the use of the bearing capacity factors (N_{c0}, N_{q0}, and $N_{\gamma 0}$) and the depth factors (F_{cd}, F_{qd}, and $F_{\gamma d}$) is both convenient and accurate.

6. The proposed rigorous solutions of the bearing capacity factors (N_{c0}, N_{q0}, and $N_{\gamma 0}$) and the depth factors (F_{cd}, F_{qd}, and $F_{\gamma d}$) are useful and they can be used by pratising engineers to evaluate bearing capacity requirements of caissons in cohesive-frictional soils with great confidence.

The results in this study are applicable to skirted circular footing subjected to drained loading. For the open caissons which are generally sunken within the ground and have an opening at the bottom and top

(during sinking), the current drained solutions may not be suitable. In addition, the interface between caissons and soils is only set to be fully rough, where the adhesion factor is set to be one. The influence of the adhesion factor on the bearing capacity factors may be significant, and future works should consider the full range of the adhesion factor (0 to 1) for more realistic simulations.

Data Availability Some or all data, models, or code that support the findings of this study are available from the corresponding author upon reasonable request.

Declarations

Conflict of interest The authors have not disclosed any competing interests.

References

Al-Aghbari MY, Dutta RK (2008) Performance of square footing with structural skirt resting on sand. Geomech Geoeng 3(4):271–277

Al-Aghbari MY, Mohamedzein YEA (2004) Bearing capacity of strip foundations with structural skirts. Geotech Geol Eng 22:43–57

Andersen KH, Dyvik R, Schroder K, Hansteen OE, Bysveen S (1993) Field test of anchors in clay II: predictions and interpretation. J Geotech Geoenviron Eng 119:1532–1549

Bransby MF, Yun G (2009) The undrained capacity of skirted strip foundations under combined loading. Géotechnique 59(2):115–125

Cauble DF (1996) Experimental measurements for a model suction caisson. Ph.D. thesis. Massachusetts Institute of Technology, USA

Chavda JT, Dodagoudar GR (2019) Finite element evaluation of vertical bearing capacity factors Nc′, Nq′ and Nγ′ for ring footings. Geotech Geol Eng 37(2):741–754

Clukey EC, Morrison MJ (1993) A centrifuge and analytical study to evaluate suction caissons for TLP applications in Gulf of Mexico. In: Design and performance of deep foundation ASCE, pp 141–56

Deng Z, Wang C, Yao Y et al (2020) Numerical simulation of an oscillating water column device installed over a submerged breakwater. J Mar Sci Technol 25:258–271

Dyvik R, Andersen KH, Hansen SB, Christophersen HP (1993) Field test of anchors in clay I: description. J Geotech Geoenviron Eng 119:1515–1531

Eid HT (2013) Bearing capacity and settlement of skirted shallow foundations on sand. Int J Geomech 13(5):645–652

Eid HT, Alansari OA, Odeh AM, Nasr MN, Sadek HA (2009) Comparative study on the behavior of square foundations resting on confined sand. Can Geotech J 46(4):438–453

Geer M (1996) Analysis of pile and suction caisson behavior in axial loading. Ph.D. thesis. Massachusetts Institute of Technology, USA

Gourvenec S (2008) Effect of embedment on the undrained capacity of shallow foundations under general loading. Géotechnique 58(3):177–185

Gourvenec S, Barnett S (2011) Undrained failure envelope for skirted foundations under general loading. Géotechnique 61(3):263–270

Keawsawasvong S, Lawongkerd J (2021) Influences of anisotropic undrained shear strengths of clays on pullout capacity of planar caissons. Sci Technol Asia 26(3):90–98

Keawsawasvong S, Ukritchon B (2016) Finite element limit analysis of uplift capacity of planar caissons in clay. Comput Geotech 75:12–17

Keawsawasvong S, Ukritchon B (2017a) Finite element analysis of undrained stability of cantilever flood walls. Int J Geotech Eng 11(4):355–367

Keawsawasvong S, Ukritchon B (2017b) Undrained lateral capacity of I-shaped concrete piles. Songklanakarin J Sci Technol 39(6):751–758

Keawsawasvong S, Ukritchon B (2020) Design equation for stability of shallow unlined circular tunnels in Hoek-Brown rock masses. Bull Eng Geol Environ 79:4167–4190

Keawsawasvong S, Ukritchon B (2021) Undrained stability of plane strain active trapdoors in anisotropic and non-homogeneous clays. Tunn Undergr Space Technol 107:103628

Keawsawasvong S, Yoonirundorn K, Senjuntichai T (2021) Uplift capacity factor for cylindrical suction caissons in anisotropic clays based on anisotropic undrained shear failure criterion. Transp Infrastruct Geotechnol 8(4):629–644

Khatri VN, Kumar J (2019) Finite-element limit analysis of strip and circular skirted footings on sand. Int J Geomech 19(3):06019001

Khatri VN, Debbarma SP, Dutta RK, Mohanty B (2017) Pressure-settlement behavior of square and rectangular skirted footings resting on sand. Geomech Eng 12(4):689–705

Krabbenhoft K, Lyamin AV, Sloan SW (2007) Formulation and solution of some plasticity problems as conic programs. Int J Solids Struct 44(5):1533–1549

Krabbenhoft K, Lyamin A, Krabbenhoft J (2015) Optum computational engineering (OptumG2). http://www.optumce.com

Kumar J, Khatri VN (2011) Bearing capacity factors of circular foundations for a general c–ϕ soil using lower bound finite elements limit analysis. Int J Numer Anal Methods Geomech 35(3):393–405

Lai F, Liu S, Deng Y, Sun Y, Wu K, Liu H (2020) Numerical investigations of the installation process of giant deep-buried circular open caissons in undrained clay. Comput Geotech 118:103322

Lai F, Zhang N, Liu S, Sun Y, Li Y (2021) Ground movements induced by installation of twin large diameter deeply-buried caissons: 3D numerical modeling. Acta Geotech 16:2933–2961

Lyamin AV, Sloan SW (2002a) Lower bound limit analysis using non-linear programming'. Int J Numer Methods Eng 55(5):573–611

Lyamin AV, Sloan SW (2002b) Upper bound limit analysis using linear finite elements and non-linear programming. Int J Numer Anal Methods Geomech 26(2):181–216

Lyamin AV, Salgado R, Sloan SW, Prezzi M (2007) Two- and three-dimensional bearing capacity of footings in sand. Geotechnique 57(8):647–662

Mana DSK, Gourvenec S, Martin CM (2013) Critical skirt spacing for shallow foundations under general loading. J Geotech Geoenviron Eng 139:1554–1566

Martin CM (2004) ABC—analysis of bearing capacity. www.civilengoxacuk/people/cmm/software/abc

Mello PC, Malta EB, da Silva ROP et al (2021) Influence of heave plates on the dynamics of a floating offshore wind turbine in waves. J Mar Sci Technol 26:190–200

Meyerhof GG (1963) Some recent research on the bearing capacity of foundations. Can Geotech J 1(1):16–26

O'Dwyer KG, McCabe BA, Sheil BB, Hernon DP (2018). Blackpool south strategy project: analysis of pipe jacking records. In: Proceedings of Civil Engineering Research in Ireland (CERI 2018), Dublin, Ireland

O'Dwyer KG, McCabe BA, Sheil BB (2020) Interpretation of pipe-jacking and lubrication records for drives in silty sand. Undergr Space 5(3):199–209

OptumCE (2021) OptumG2. Optum Computational Engineering, Copenhagen. See https://optumce.com/. Accessed 25 June 2021

Randolph M, Gourvence S (2011) Offshore geotechnical engineering. Taylor & Francis

Sales LA, Patricio AR, Morooka CK (2021) A selection method of offshore production systems considering uncertainties. J Mar Sci Technol. https://doi.org/10.1007/s00773-021-00811-3

Shiau J, Al-Asadi F (2020a) Twin tunnels stability factors Fc, Fs and Fr. Geotech Geol Eng. https://doi.org/10.1007/s10706-020-01495-z

Shiau J, Al-Asadi F (2020b) Determination of critical tunnel heading pressures using stability factors. Comput Geotech 119:103345

Shiau J, Al-Asadi F (2020c) Three-dimensional heading stability of twin circular tunnels. Geotech Geol Eng 38(3):2973–2988

Shiau J, Al-Asadi F (2020d) Three-dimensional analysis of circular tunnel headings using Broms and Bennermark's original stability number. Int J Geomech 20(7):06020015

Shiau J, Al-Asadi F (2021) Revisiting circular tunnel stability using Broms and Bennermarks' original stability number. Int J Geomech 21(5):06021009

Shiau J, Smith C (2006) Numerical analysis of passive earth pressures with interfaces. In: Proceedings of the III European Conference on Computational Mechanics (ECCM 2006), 5–8 June 2006, Lisbon, Portugal

Shiau JS, Lyamin AV, Sloan SW (2016a) Application of pseudo-static limit analysis in geotechnical earthquake design. In: 6th European conference on numerical methods in geotech. eng., Graz, Austria

Shiau J, Lamb B, Sams M (2016b) The use of sinkhole models in advanced geotechnical engineering teaching. Int J Geomate 10(2):1718–1724

Shiau J, Sams M, Lamb B (2016c) Introducing advanced topics in geotechnical engineering teaching–tunnel modelling. Int J Geomate 10(1):1698–1705

Shiau J, Lee JS, Al-Asadi F (2021a) Three-dimensional stability analysis of active and passive trapdoors. Tunn Undergr Space Technol 107:103635

Shiau J, Chudal B, Mahalingasivam K, Keawsawasvong S (2021b) Pipeline burst-related ground stability in blowout condition. Transp Geotech 29:100587

Sloan SW (1988) Lower bound limit analysis using finite elements and linear programming. Int J Numer Anal Methods Geomech 12(1):61–77

Sloan SW (1989) Upper bound limit analysis using finite elements and linear programming. Int J Numer Anal Methods Geomech 13(3):263–282

Sloan SW (2013) Geotechnical stability analysis. Géotechnique 63(7):531–572

Terzaghi K (1943) Theoretical soil mechanics. Wiley, New York

Ukritchon B, Keawsawasvong S (2016) Undrained pullout capacity of cylindrical suction caissons by finite element limit analysis. Comput Geotech 80:301–311

Ukritchon B, Keawsawasvong S (2017a) Error in Ito and Matsui's limit equilibrium solution of lateral force on a row of stabilizing piles. J Geotech Geoenviron Eng 143(9):02817004

Ukritchon B, Keawsawasvong S (2017b) Unsafe error in conventional shape factor for shallow circular foundations in normally consolidated clays. J Geotech Geoenviron Eng 143(6):02817001

Ukritchon B, Keawsawasvong S (2019a) Design equations of uplift capacity of circular piles in sands. Appl Ocean Res 90:10184

Ukritchon B, Keawsawasvong S (2019b) Stability of retained soils behind underground walls with an opening using lower bound limit analysis and second-order cone programming. Geotech Geol Eng 37(3):1609–1625

Ukritchon B, Keawsawasvong S (2020a) Undrained lower bound solutions for end bearing capacity of shallow circular piles in non-homogeneous and anisotropic clays. Int J Numer Anal Methods Geomech 44(5):596–632

Ukritchon B, Keawsawasvong S (2020b) Undrained stability of unlined square tunnels in clays with linearly increasing anisotropic shear strength. Geotech Geol Eng 38(1):897–915

Ukritchon B, Wongtoythong P, Keawsawasvong S (2018) New design equation for undrained uplift capacity of suction caissons considering combined effects of caisson aspect ratio, adhesion factor at interface, and linearly increasing strength. Appl Ocean Res 75:1–14

Ukritchon B, Yoang S, Keawsawasvong S (2019) Three-dimensional stability analysis of the collapse pressure on flexible pavements over rectangular trapdoors. Transp Geotech 21:100277

Ukritchon B, Yoang S, Keawsawasvong S (2020) Undrained stability of unsupported rectangular excavations in non-homogeneous clays. Comput Geotech 117:103281

Wakil AZEL (2013) Bearing capacity of Skirt circular footing on sand. Alex Eng J 52(3):359–364

Yodsomjai W, Keawsawasvong S, Senjuntichai T (2021) Undrained stability of unsupported conical slopes in anisotropic clays based on Anisotropic Undrained Shear failure criterion. Transp Infrastruct Geotechnol 8(4):557–568

Yun G, Bransby MF (2007) The undrained vertical bearing capacity of skirted foundations. Soils Found 47(3):493–505

Zhao L, Wang JH (2008) Vertical bearing capacity for ring footings. Comput Geotech 35(2):292–304